Journal of Neonatal Surgery
ISSN(Online): 2226-0439
Vol. 14, Issue 8 (2025)
https://www.jneonatalsurg.com

OPEN ACCESS

Enhanced (CuO/ZnO) Nanocomposites Synthesized via Thermal Evaporation for High-Performance Photodetector Applications

Ahmed A. Jabber[1], Ali R. Abdulridha[2]

[1,2]Department of Physics, College of Education for Pure Sciences, University of Babylon, Babylon 51002, Iraq.

Cite this paper as: Ahmed A. Jabber, Ali R. Abdulridha, (2025) Enhanced (CuO/ZnO) Nanocomposites Synthesized via Thermal Evaporation for High-Performance Photodetector Applications. *Journal of Neonatal Surgery*, 14 (8), 346-363.

ABSTRACT

In this article, thin films of copper oxide (CuO) doped with zinc oxide (ZnO) were produced using thermal evaporation at 1×10^{-7} bar pressure and 0.5 nm/s deposition rate. Deposition on glass substrates yielded a 50±0.2 nm film thickness at ambient temperature. After annealing at 400 ^{0}C for two hours, XRD examination revealed a monoclinic wurtzite structure of CuO. AFM investigation found a 54.46% increase in surface roughness, a 52.5% increase in RMS, and a 27.5% average particle size with increasing ZnO concentration. FE-SEM and EDX confirmed the uniform distribution of Cu, Zn, O, and CuO/ZnO nanocomposites. Higher ZnO improved absorption, refractive index, and extinction coefficient; energy band gap fell from 3.601 to 3.388 eV. Electrical studies showed enhanced DC conductivity, resistance, and activation energy with higher ZnO concentration and temperature. I–V tests showed greater photocurrent, responsiveness, and sensitivity, making these films promising for optoelectronic and photodetector applications.

Keywords: *Copper oxide, Nanocomposites, Photodetector, Thermal evaporation, Thin films, Zinc oxide.*

1. INTRODUCTION

The materials community has demonstrated significant interest in nanocomposites due to their qualities being affected by composition, morphology, and size distribution [1]. An extensive study has been conducted on nanotechnology due to the challenges it can address in development, production, and application [2]. Systems with a wide range of capabilities, enhanced sensitivity, huge surface area, strain resistance, catalytic properties, and novel surface effects are all within reach thanks to nanotechnology. There are a plethora of properties associated with the size of small nanocomposites [3].

Nanotechnology involves the reengineering of materials and devices through atomic-level manipulation of matter [4]. Nanotechnology is primarily influenced by advancements in foundational chemistry and physics research [5]. Applications of nanotechnology are utilized throughout nearly all scientific and technical domains [6]. Metal oxides exhibit considerable utility in various applications owing to their intrinsic capacity for effective light absorption [7]. Therefore, metal oxide nanocomposites must be deposited on organic substrates like glass. Metal and metal oxide nanocomposites are used in ecological cleanup, detection at the molecular level, and catalysis [8].

Oxides of metals have been investigated in favor of numerous purposes [9]. The distinct physical and chemical features of nanocomposites render them a subject of significant interest. The characteristics of enhanced damping in nanocomposites, among its distinguishing characteristics, are improved strength, mechanical stability, and better heat conductivity [10]. Metal oxide nanocomposites with high surface area have garnered significant interest for scientific research due to their potential in optical electronics, sensing devices, and nanoelectronics [11]. Diverse semiconductor materials are fundamental to the electronics industry, encompassing computer technology, energy conversion, and sensor fabrication. Recent initiatives focus on reducing the dimensions of semiconductor-based devices to the nanoscale [12].

Transition metal oxides, including those of elements such as copper, iron, nickel, and cobalt, are widely utilized across diverse applications. ZnO, a significant semiconducting material, is regarded as an attractive nanomaterial due to its notable electro-optical, piezoelectric, and magnetic capabilities [13,14]. Owing to a substantial 3.37 eV direct band gap, a considerable 60 meV exciton binding energy, and light-transmitting capability [15], ZnO possesses significant promise for optoelectronic devices. ZnO nanostructures (NSs), characterized by their Chemical and biosensing applications, benefit from surface area relative to volume [16,17]. ZnO, an n-type semiconductor, is a viable choice for gas sensors, transparent conductors, light-emitting devices, antibacterial, and photocatalysis [18–21].

In contrast, CuO has a band gap between 3 and 3.62 eV, indicating that it is a p-type semiconductor, which is notably facile to synthesize and devoid of any ecologically detrimental components in its composition [22]. Often used as a p-type

semiconductor, CuO finds use in photodetectors, solar cells, photocatalysis, gas sensors, and related fields [23]. Because of its exceptional absorption of both visible and infrared light, as well as its non-toxicity, affordability, lack of impact on the environment, and ease of fabrication, CuO is a metal oxide that garners much interest [24]. Both zinc oxide and copper oxide are multifunctional oxides that have been widely researched for a variety of applications. Both of these oxides are biocompatible and cost-effective. A recent study emphasizes the development of using nanoscale systems composed of mixed CuO and ZnO to incorporate the aforementioned characteristics effectively [25–27], alongside the distinctive physicochemical properties resulting from their nano-organization [28,29]. Furthermore, the functional performance of nanocomposites can be improved by altering the spatial distribution of each component, as CuO/ZnO contacts create p-n heterojunctions that facilitate charge separation [30]. The development of adaptable synthetic methods for CuO/ZnO nanoarchitectures, particularly under mild circumstances to avert the production of ternary Cu-Zn-O phases, presents a significant and ongoing problem [31].

There has been a surge of interest in creating APDs, quantum well detectors, photoconductors, photodiodes, and phototransistors in recent years [32]. Photodetectors make use of materials including Ge: Cu as the active components, Si, InAs, SiC, InP, Ge, and InGaAs, [33]. The pursuit of cost-effective alternative materials has become increasingly significant during the past twenty years. Metal oxides have grown in significance because of their affordability, stability, simplicity of production, and compatibility with both semiconductors and metals [34].

In this research, the current work is concerned with studying the effect of ZnO doping on the characteristics of CuO films such as morphological, structural, electrical, and optical, formed on a glass substrate via thermal evaporation, for UV photosensor applications.

2. EXPERIMENTAL PROCEDURES

This section addresses the procedural elements related to the fabrication and analysis of undiluted CuO thin films doped with varying concentrations of ZnO (0.08, 0.14, and 0.20 wt.%) via the thermal evaporation method at RT. The 50-nm films were deposited on glass substrates and annealed at 400 ^{0}C. The spectris analytical X-ray diffractometer, which uses Cu Kα radiation, was used to capture X-ray diffraction (XRD) patterns. A transmission electron microscope with an Accelerating FE-SEM voltage range of 200V to 30 kV. Analysis of the nanocomposites' microstructure was carried out using an atomic force microscope (AFM). Optical. Thin film optical measurements include absorbance (A), coefficient of absorption (α), the extinction coefficient (k_o), the refractive index (n), the optical energy gap (E_g), and optical conductivity (σ_{op}). A Shimadzu UV-1800 dual-beam laser spectrophotometer measured 200-1100 nm. The electrical properties of DC thin films were examined. Keithley-2400 electrometers measured the temperature. The current-voltage (I-V) characteristic for both dark and illumination, the photocurrent (μA), and time(s) in light intensity (26 m W/cm^2) are the measurements used for the thin film photodetector.

Relaying on the wave diffusion direction, the coefficient of absorption is the percentage by which the energy flow of an incoming ray decreases with respect to a unit distance. The type of electronic transitions, photon energy, and material qualities all have an impact on the absorption coefficient (α). The following equation may be used to find it [35]:

$$\alpha = 2.303\ (\frac{A}{t}) \quad (1)$$

Above the valence band and between the conduction band (C.B.), the transmission takes place. The optical band gap (E_g^{opt}) was determined using the Tauc plot model, based on the following relation [36]:

$$\alpha h\upsilon = B\ \left(h\upsilon - E_g^{opt}\right)^r \quad (2)$$

The temperature dependency of electrical conductivity was examined by the Arrhenius equation, elucidating the thermal activation characteristics of charge carriers. The connection is articulated as [37]:

$$\sigma_{D.C.} = \sigma_o \exp - (E_{act}/K_B T) \quad (3)$$

In this case, σ represents electrical conductivity that is particular to temperature. Eact stands for activation energy, K_B for the Boltzmann constant, and T and σ_o for electrical conductivity at absolute zero.

Key metrics for assessing Responsivity (R), sensitivity (S), and quantum efficiency (QE) are the three characteristics that determine the performance of photodetectors and detectivity (D*) [38];

$$R_\lambda = \frac{I_{ph}}{A\ E_{opt}} \quad (4)$$

$I_{ph} = I_{light} - I_{dark}$ measures the photocurrent (A), where the effective area of the device (A) in (m²), and E_{opt} signifies the incident light output (W/m²). The sensitivity is defined by [39]:

$$S(\%) = \frac{I_{light} - I_{dark}}{I_{dark}} \quad (5)$$

Quantum efficiency is given by [38]:

$$QE = \frac{hc}{q_e \lambda} R_\lambda \quad (6)$$

Here, h, c, and λ are the Planck's constant, the speed of light (in m/s), and the wavelength of the incoming light respectively.

The detectivity is given by [39]:

$$D^* = \frac{R_\lambda}{\sqrt{2 q_e I_d / A}} \quad (7)$$

3. RESULTS AND DISCUSSIONS

3.1 X–ray Diffraction Analysis

Separate XRD patterns of diffraction for the thin films of ZnO and CuO are presented in Figure 1. Figure 2 displays the patterns of XRD of CuO and ZnO-doped CuO films following annealing at 400 °C. The spectrum exhibits one peak at 35.55° (-111) corresponding to CuO (as per JCPDS card No. 96-901-5925), indicating that the crystal structure of CuO is monoclinic wurtzite-type, with the crystals aligned along the c-axis [40]. CuO with different ratios of ZnO showed 2θ at 56.53° (110) associated. It is possible to index the diffraction patterns to the hexagonal wurtzite phase, which corresponds to (marked peaks, as per JCPDS card No. 96-900-4180). This shows that both undoped and doped CuO Films produced by thermal evaporation processes demonstrate a consistent trend of enhanced film crystallinity; the results demonstrate the increase in peak intensity with increasing ZnO content. This investigation is closely reported by [40].

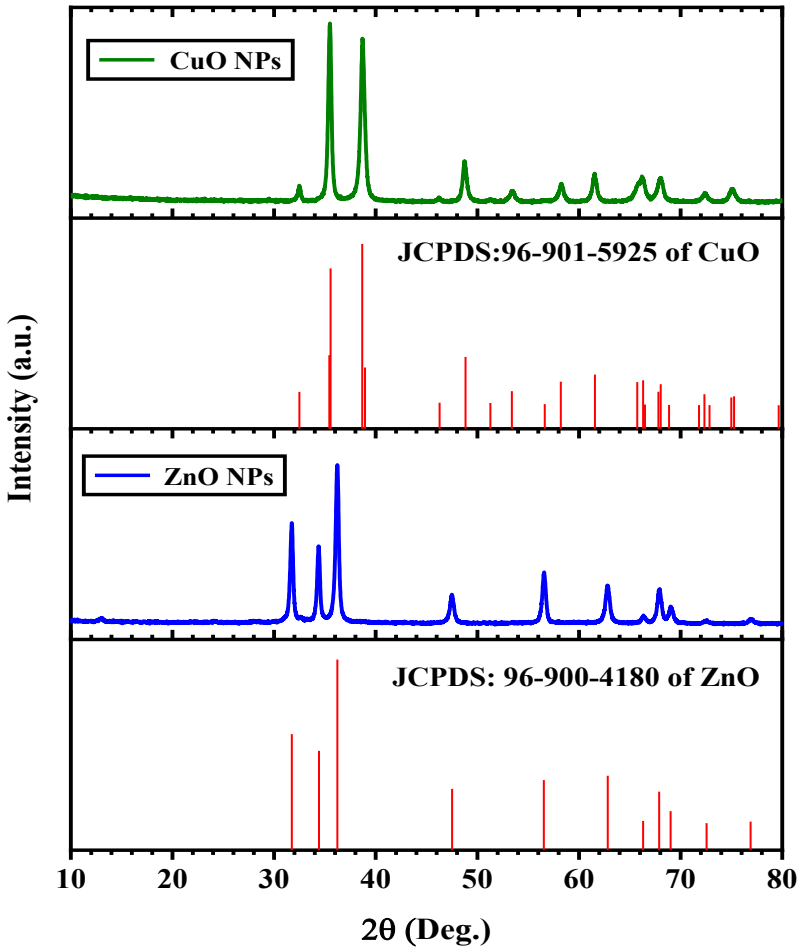

Figure 1 XRD of CuO and ZnO nano-films for individually.

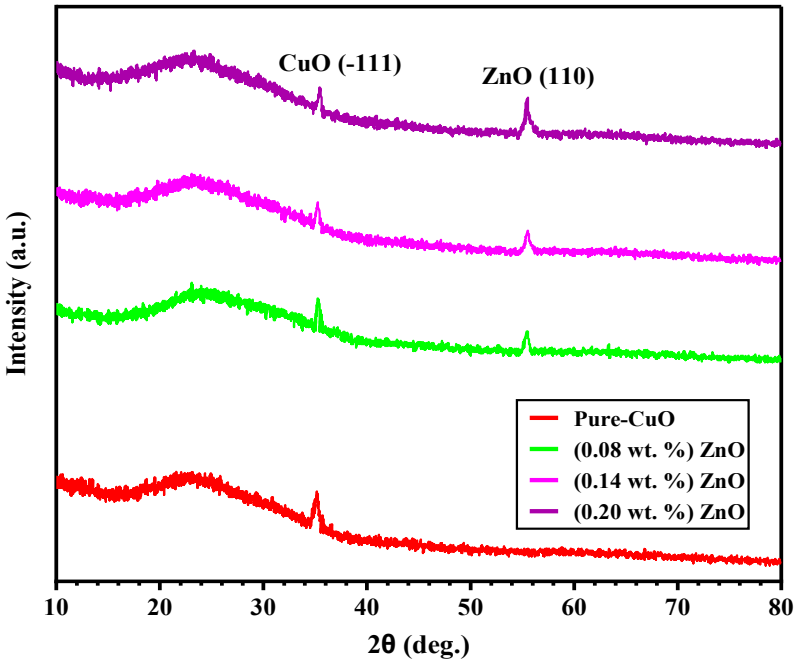

Figure 2 Plot of XRD analysis for (CuO/ZnO) thin films at 400 °C.

3.2 Atomic Force Microscope (AFM) Measurements of (CuO/ZnO) Nanocomposites

Figure 3 presents AFM images depicting a 6 × 6 μm² scan area was utilized, using four layers of CuO/ZnO thin films deposited on glass substrates. During the annealing process at 400 °C, a rise in the concentration of ZnO nanocomposites in the films results in enhanced crystallinity and bigger grain sizes. As the concentration of ZnO nanocomposites escalates from (0.08 to 0.20) wt.%, the picture of AFM shows that the average grain width expands from 858 nm for pure CuO to 1184 nm for ZnO thin films at 0.20 wt.%. Table 1 summarizes the root-mean-square (RMS) and the roughness of the films' surface values, where the RMS roughness escalates from 39.8 to 83.8 nm due to an augmentation in the concentration of ZnO nanocomposites as discussed and explained in [41,42].

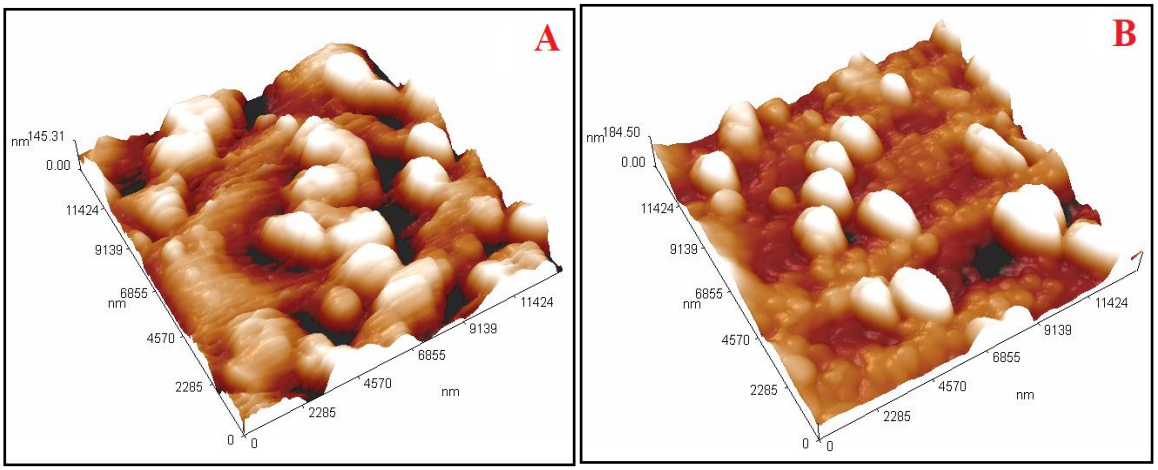

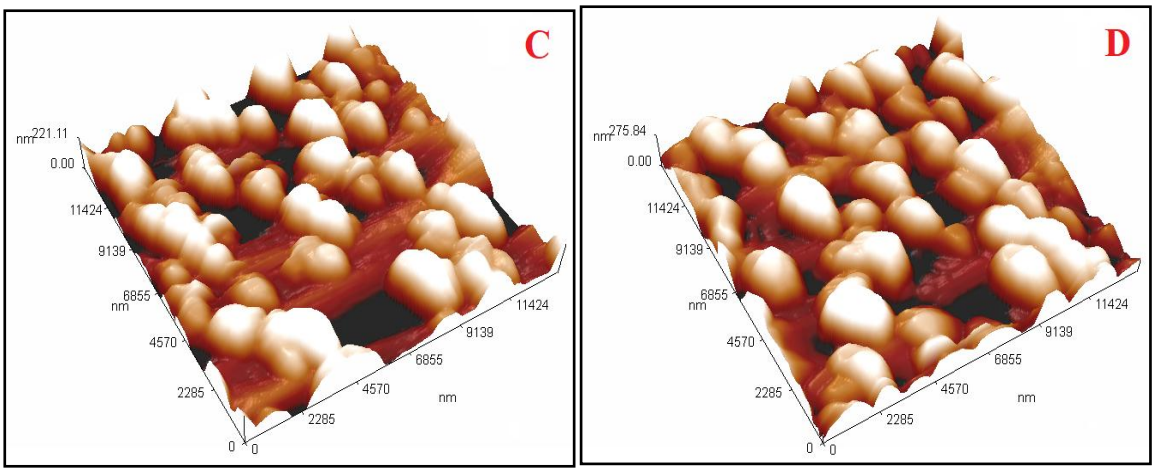

Figure 3 AFM surface morphology of (CuO/ZnO) NCs: A: pure CuO annealing 400 ^{0}C, B: (0.08 wt.%) ZnO NPs, C: (0.14 wt.%) ZnO NPs, D:(0.20 wt.%) ZnO NPs.

Table 1 Morphological characteristics of 400 ^{0}C-annealed (CuO/ZnO) thin films.

ZnO-doped CuO (wt.%)	Root mean square Sq (nm)	Roughness average Sa (nm)	Ten-point heigh Sz (nm)	Average Diameter (nm)
Pure (CuO)	39.8	32.6	144	858
0.08 wt.% ZnO	44.2	34.2	156	1053
0.14 wt.% ZnO	68.7	58.5	167	1182
0.20 wt.% ZnO	83.8	71.6	210	1184

3.3 Scanning Electron Microscope (FESEM)

Using Scanning electron microscopy (FESEM) at 500 nm, the Surface morphology of (CuO/ZnO) thin films was observed. Electron Microscopy examined the ZnO nanoparticle surface shape and size. The FESEM picture revealed the presence of both individual ZnO nanocomposites and a significant quantity of aggregates. Figure 4 shows nanocomposites in thin films under study. At lower chemical concentrations, nanocomposites aggregate, explaining these observations. CuO nanocomposites can promote the formation of a network when there is a greater interaction with ZnO nanocomposites. Initially, the size of the nanocomposites decreases as the ZnO content increases, but it subsequently increases with further ZnO addition. The arrangement of particles indicates the presence of co-granular structures.

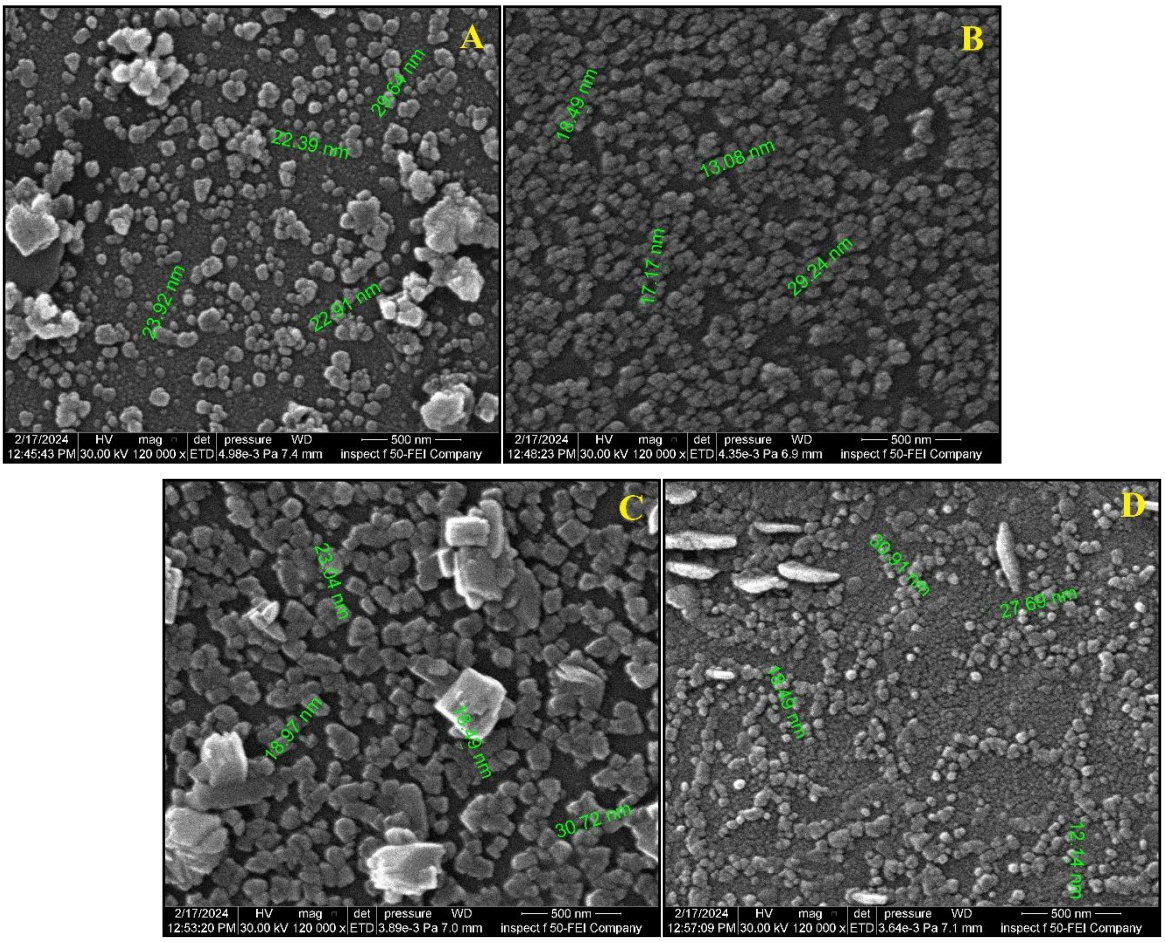

Figure 4 FESEM images of (CuO/ZnO) NCs: A: pure CuO, B:(0.08wt.%) ZnO, C:(0.14 wt.%) ZnO, D:(0.20 wt.%) ZnO for annealing 400 ^{0}C.

1.2 Energy Dispersive X-ray Spectroscopy (EDX)

The elemental compositions of synthesized samples were determined by EDX, and from the table accompanying the spectrum in Figure 5, the EDX of the Zn-CuO samples all have spectra that reveal that Zn, Cu, and O are present. Furthermore, there is no further peak that confirms the synthesized Zn CuO samples' purity by revealing the presence of unexpected components (H, S, and C) as discussed in [43]. The composition of copper, zinc, and oxygen was determined for the CuO–CuO-ZnO nanocomposite synthesized by different concentrations (Pure, 0.08, 0.14, and 0.20) wt.% ZnO. In Pure (CuO), the composition was found to be 56.9% Cu, 43.1% O in 0.08 wt.% ZnO, the composition was 44.9% Cu, 1.8% Zn, and 53.3% O in 0.14 wt.% ZnO, the composition included 48.6% Cu, 3.1% Zn, and 48.4% O, and in 0.20 wt.% ZnO, the composition included 41.2% Cu, 4.6% Zn, and 54.2% O as discussed in [44]. When different concentrations of zinc oxide were added, a shift in energy of 5 eV was observed.

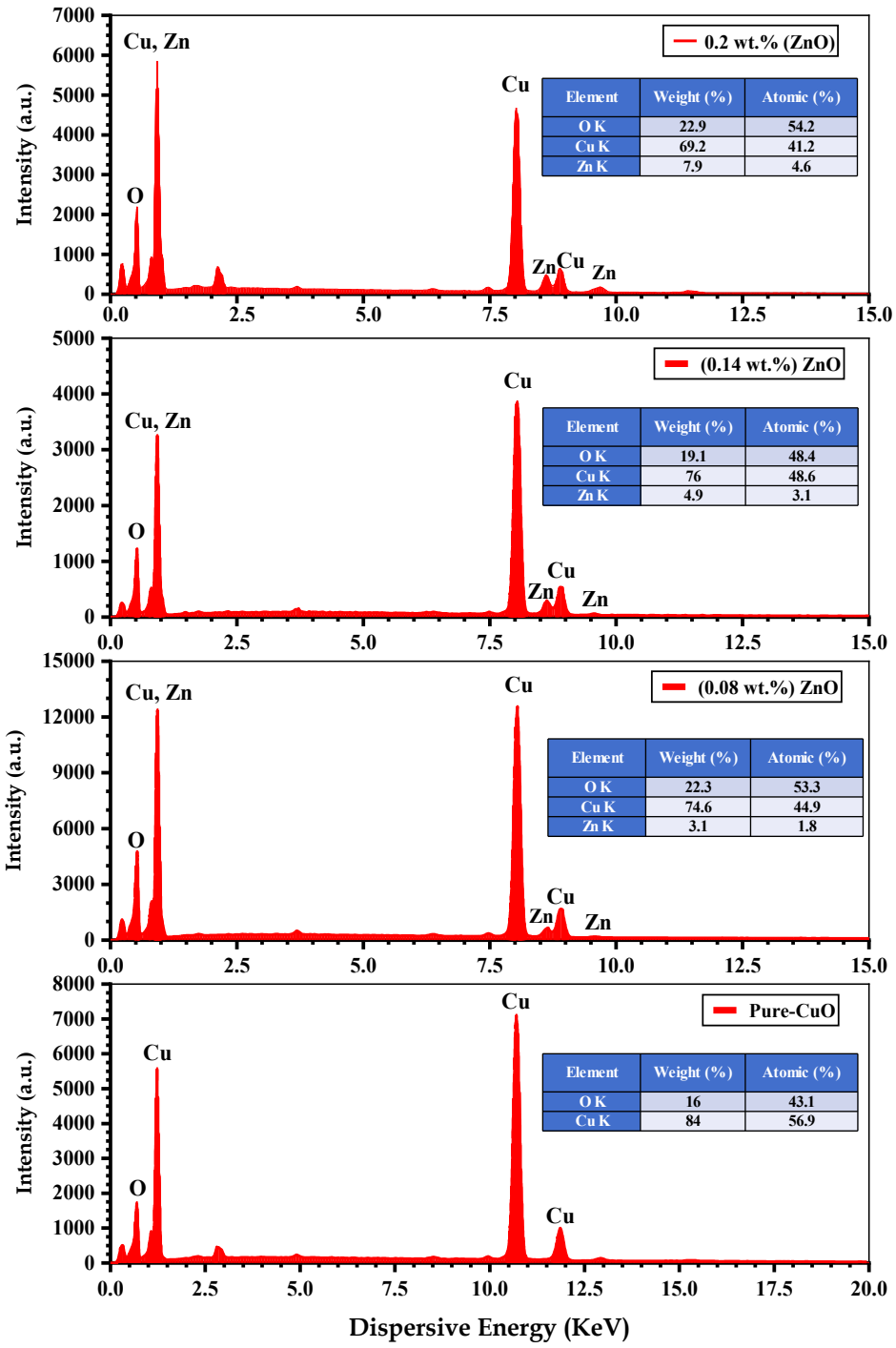

Figure 5 the EDX spectrum of CuO/ZnO nano-films.

3.4 Optical Characteristics of (CuO/ZnO) Nanocomposites

Figure 6 illustrates the ultraviolet-visible spectra of the ZnO and CuO nanocomposites that were produced. All samples were tested for absorbance between 320 and 720 nm. Factors such as impurity centers, particle size, oxygen vacancies, micro-strain, dislocation density, and layer thickness influence nanomaterial absorbance as discussed and explained in [43]. CuO/ZnO absorption with variable concentration (ZnO) and wavelength range at normal temperature. (CuO/ZnO) optical absorption varies with wavelength, as shown in Figure 6. These statistics imply that all films have higher UV absorption spectra. The nanocomposites exhibit a noticeable lack of absorbance in the visible spectrum. To provide further elucidation, we can approach this matter from the following perspective: Photons of high frequencies do not undergo interactions with atoms, resulting in their transmission rather than obstruction. Substances around the fundamental absorption edge absorb

photons as the light wavelength decreases. An increase in the proportion of ZnO by weight improves absorption. The absorption of light by unbound electrons causes this to occur. The findings are consistent with those of previous studies [45].

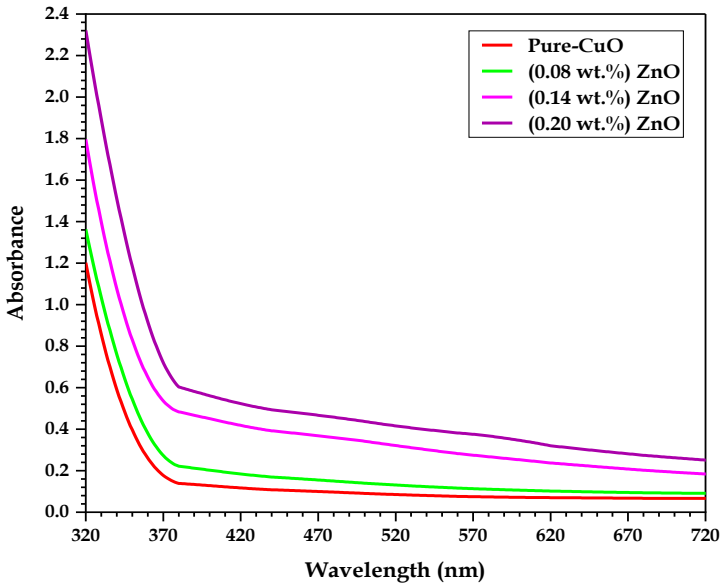

Figure 6 shows the absorbance spectra for (CuO/ZnO) thin films as a function of wavelength.

Figure 7 illustrates the coefficient of absorption in relation to the CuO/ZnO thin films case. At levels of lower energy, the coefficient of absorption is the lowermost at longer wavelengths. An electron within a semiconductor, either as an atom or an ion. Since photon absorption requires energy equal to or greater than the band gap, photons with insufficient energy fail to excite electrons from the valence band to the conduction band, resulting in limited optical absorption and suppressed generation of charge carriers [46]. Maximizing high-energy absorption increases the probability of electron transitions. Consequently, the energy of the photon is adequate to enable the change in the valence band electron to the conduction band. The seen photon's energy exceeded the allowed energy limit. This coefficient runs higher than the absorption coefficient during direct electron transitions; hence, at elevated energies ($\alpha > 10^4$ cm^{-1}), electrons and photons retain their momentum and energy while traversing the transition. Low-energy values of the coefficient of absorption ($\alpha < 10^4$ cm^{-1}) are expected to result in indirect electron transmission. Phonons facilitate the maintenance of electron trajectories. The absorbance coefficient of the thin layer (CuO/ZnO) exceeds 10^4 cm^{-1}.

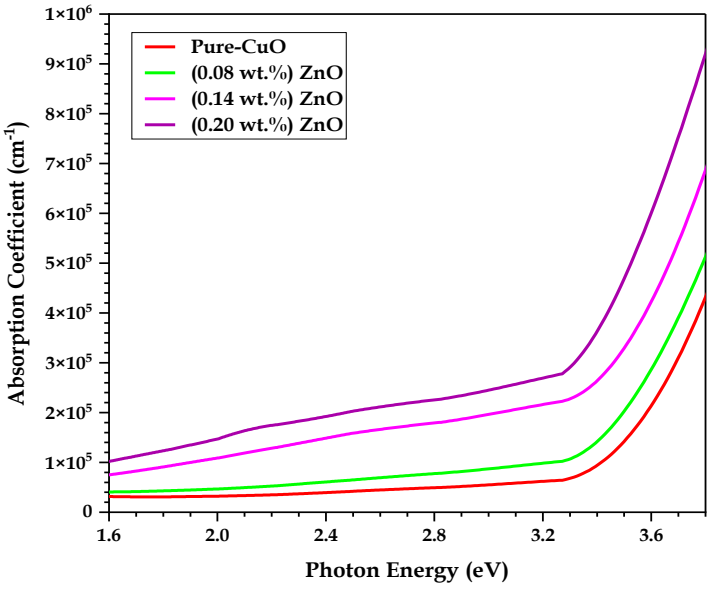

Figure 7 shows the wavelength-dependent absorption coefficient spectra of CuO/ZnO thin films.

The edge of absorption $(\alpha hv)^2$ of the material (CuO/ZnO) is depicted in Figure 8. The amount of photon energy and the

position on the upper half of the curve relationship is illustrated where the $(\alpha hv)^2 = 0$ value is obtained, moving towards x-axis. The energy gap between pure CuO and ZnO-doped CuO thicknesses of 50 nm and ratios of 0.08, 0.14, and 0.20 wt.% is shown. As the ZnO ratio grows, the energy gap decreases. The band gap values for the generated nanofilm reduced from 3.601 to 3.388 eV for allowed direct transitions and from 3.389 to 3.057 eV for authorized indirect transitions. The optical energy gap diminishes post-annealing due to the emergence of supplementary internal energy levels, the forbidden gap, and next to the conduction band. This reduction is ascribed to the heat, which decreases the energy required for direct electronic transitions and promotes the migration of charge carriers moving from the valence to the conduction band. According to these findings, there is a robust alignment with the findings of researchers [46,47], as shown in Table 2.

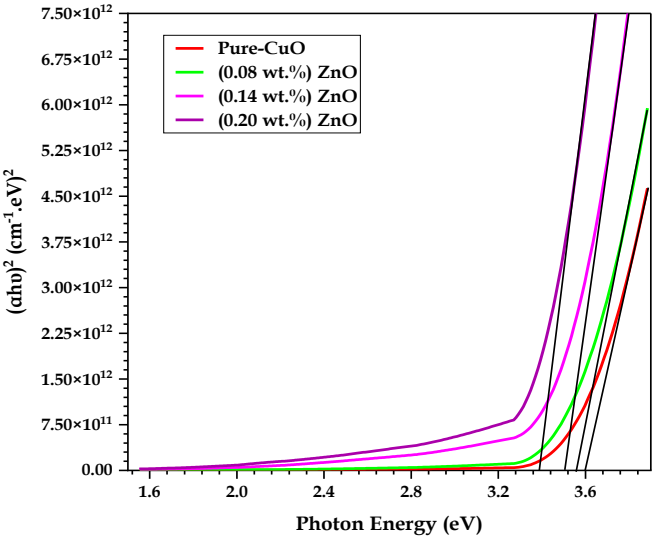

Figure 8 A plot of (αhυ) ² vs photon energy (hυ) for (CuO/ZnO) thin films at various ZnO doping ratios.

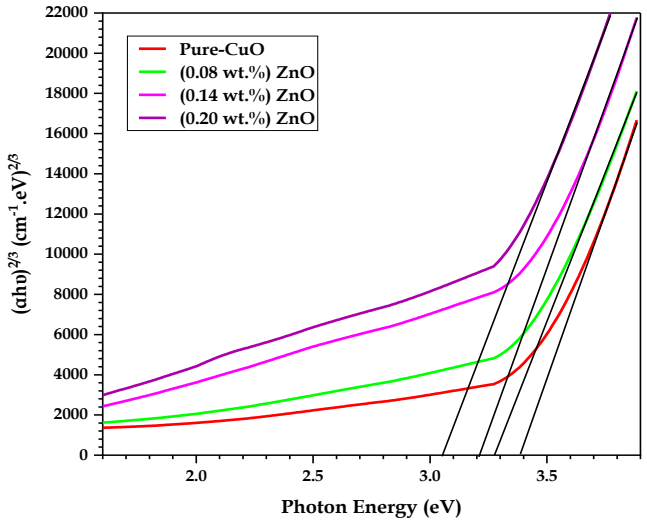

Figure 9 A plot of (αhυ) ²/³ vs photon energy (hυ) for (CuO/ZnO) thin films at various ZnO doping ratios.

Table 2 The energy gap values for both permitted and banned direct transitions in CuO/ZnO thin films.

ZnO-doped CuO (wt.%)	E_g(eV)	
	Allowed	Forbidden
Pure (CuO)	3.601	3.389
0.08 wt.%	3.562	3.278
0.14 wt.%	3.505	3.208
0.20 wt.%	3.388	3.057

The refractive index variations for (CuO/ZnO) thin films are illustrated against wavelength in Figure 10. This graph illustrates that the weight percentage increase of ZnO nanocomposites produces a higher index of refraction. The heightened density of the thin layer has been associated with this inclination. The data indicates that the refractive index of ZnO nanofilms, both pure and doped with CuO, rises as the thickness and doping of ZnO increase. The refractive index variations for (CuO/ZnO) thin films are illustrated against wavelength in Figure 10. This graph illustrates that the weight percentage increase of ZnO nanocomposites produces a higher index of refraction. The heightened density of the thin layer has been associated with this inclination. The data indicates that the refractive index of ZnO nanofilms, both pure and doped with CuO, rises as the thickness and doping of ZnO increase. The behavior can be explained by the rise in absorbance or absorption coefficient. Higher levels of doping lead to an elevation in the refractive index. Put simply, when light from an incoming source interacts with a material containing a large number of particles, the refractive index of the films is elevated. This aligns with the conclusions drawn by the researchers.

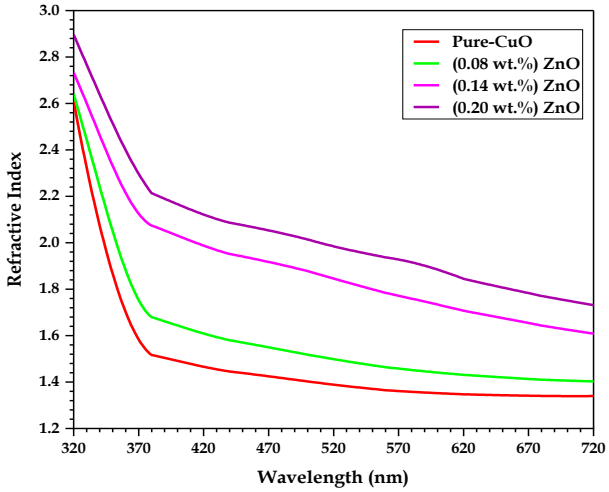

Figure 10 The refractive index spectra in respect to (CuO/ZnO) thin films wavelength.

Figure 11 shows for (CuO / ZnO) thin films the fluctuation of the wavelength-dependent extinction coefficient. The extinction coefficient (k_0) is calculated using equation (6). (k_0) exhibits a low value at a small weight% %. Nonetheless, it intensifies with the rising weight% % of nanocomposites for (ZnO). This elucidates the enhanced ZnO absorption under UV and visible light. This relates to the increased absorbance coefficient associated with higher weight percentages of ZnO nanocomposites, suggesting that ZnO ions will alter structures through interfacial locations among CuO atoms [48].

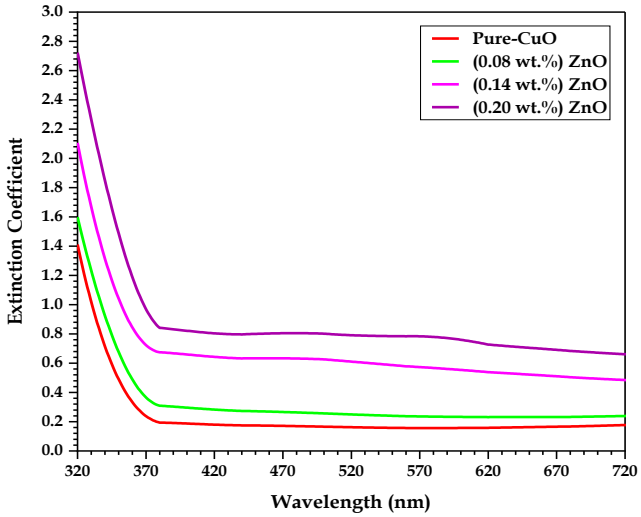

Figure 11 The extinction coefficient (k) for (CuO/ZnO) nanocomposites with wavelength.

Figure 11 shows for (CuO/ZnO) thin films the fluctuation of the wavelength-dependent extinction coefficient. (k_0) exhibits a low value at a small weight %. Nonetheless, it intensifies with the rising weight % of nanocomposites for (ZnO). This

elucidates the enhanced ZnO absorption under UV and visible light. This relates to the increased absorbance coefficient associated with higher weight percentages of ZnO nanocomposites, suggesting that ZnO ions will alter structures through interfacial locations among CuO atoms [49,50].

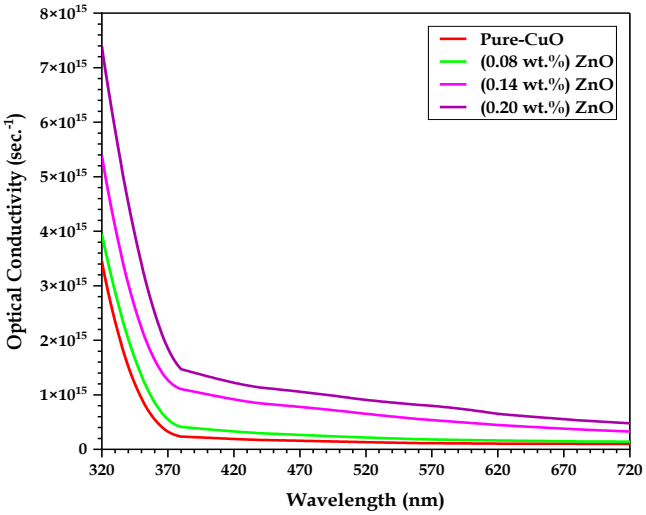

Figure 12 The optical conductivity spectra of (CuO/ZnO) thin films composed in relation to wavelength.

3.5 Direct Current (D.C) Electrical Characteristics of (CuO/ZnO) Thin Films

A thin layer of (CuO/ZnO) is shown in Figure 13 to have an electrical conductivity that varies with temperature. These numbers lead us to believe that conductivity increases as the temperature rises. Because (ZnO) molecules may entrap charge carriers in motion during a hopping process, the resistance drops as the temperature increases; so, the material's resistance is negatively connected to temperature, as shown by the negative thermal coefficient of resistance. Because the adjacent charge carriers are freed, the conductivity of (CuO/ZnO) thin films is improved. The improvement is due to the strengthening of charge carriers. In line with what other experts have found [51].

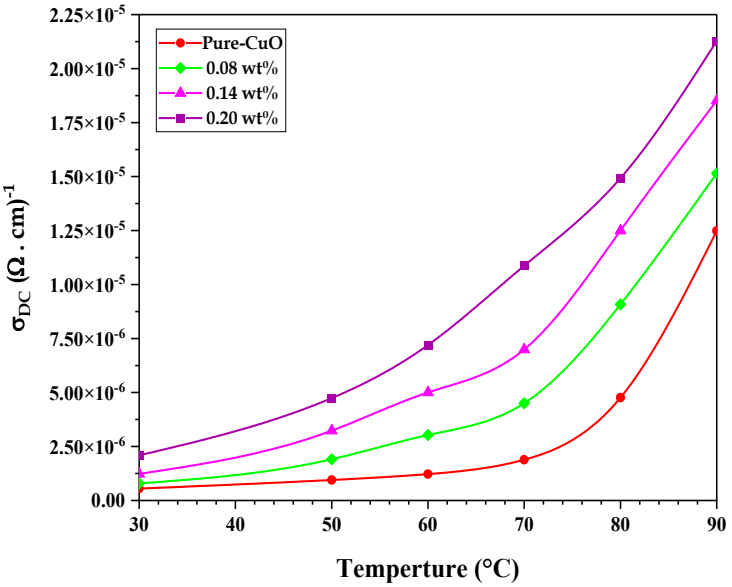

Figure 13 depicts the correlation between temperature and the thin-film electrical conductivity of direct current (D.C.) comprised of CuO/ZnO nanostructures.

Figure 14 depicts the correlation between the ZnO nanoparticle concentration in samples and the samples' electrical conductivity surface when exposed to direct current. The study results show a positive relationship between direct current electrical conductivity and ZnO concentration. This results from a persistent network of zinc oxide (ZnO) nanocomposites

forming inside the thin layers. These nanocomposites possess channels that facilitate the movement of charge carriers inside the material, accounting for this outcome. ZnO nanocomposites can enhance conductivity by improving the connectivity between CuO particles and increasing the charge carrier density. The increase in filler material is directly correlated with the growth in the number of charge transporters [52].

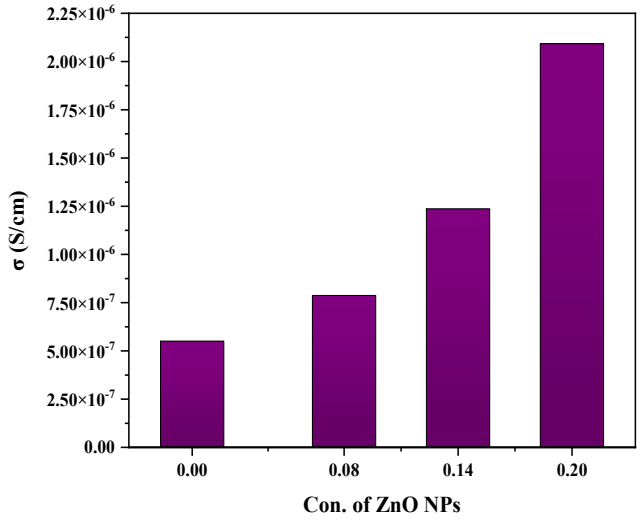

Figure 14 depicts the correlation between the ZnO nanoparticle concentration and the thin-film electrical conductivity of direct current (D.C.) comprised of CuO/ZnO nanostructures.

This relationship between the absolute temperature of the and the natural-logarithm of the standard deviation of direct current conductivity (Ln $\sigma_{D.C}$) (CuO/ZnO) nanofilms is shown in Figure 15 [53]. When plotting Ln $\sigma_{D.C}$ vs. 1000/T a straight line with a negative slope is obtained, indicating that conductivity increases with increasing temperature, as expected in semiconductors. Based on the line's slope, the activation energy Ea. It can be calculated, which reflects the energy required for electron or hole transport in the material. Changes in the slope at different temperature regions may indicate a shift in the conduction mechanism, like a change in the mechanism from band conduction to hopping conduction. We conclude that the relationship between Ln($\sigma_{D.C}$) and 1/T in CuO/ZnO nano-films reflects semiconductor behavior, where conductivity increases with temperature. This relationship may be influenced by ZnO concentration, leading to variations in electronic conduction mechanisms, particularly in nanostructured or amorphous films.

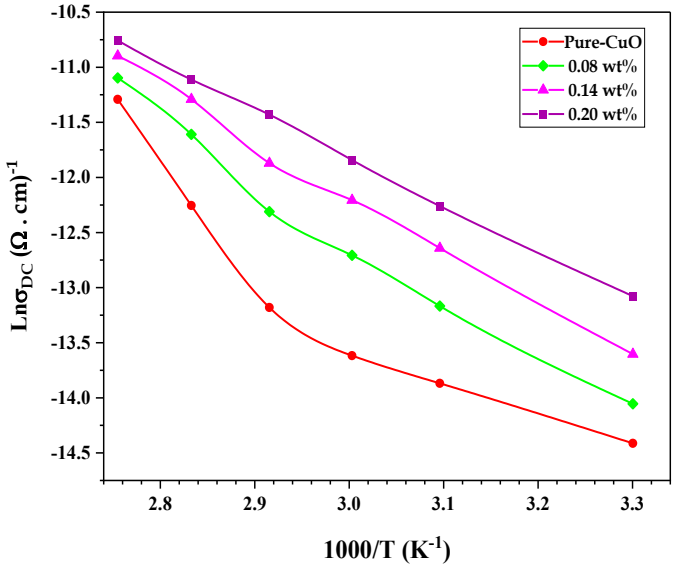

Figure 15 The correlation between the natural logarithm of electrical conductivity (Lnσ) and the absolute temperature reciprocal of thin films of (CuO/ZnO).

Figure 16 displays that the activation energy could be approximated by equation (3). According to the experimental findings, the (CuO/ZnO) thin film activation energy values ranging from 0.468 eV to 0.368 eV. Furthermore, it has been shown that when nanoparticle concentrations in thin films increase, the activation energies drop. The development of localized energy levels that serve as charge carrier traps within the energy gap is the cause of this phenomenon [54,55].

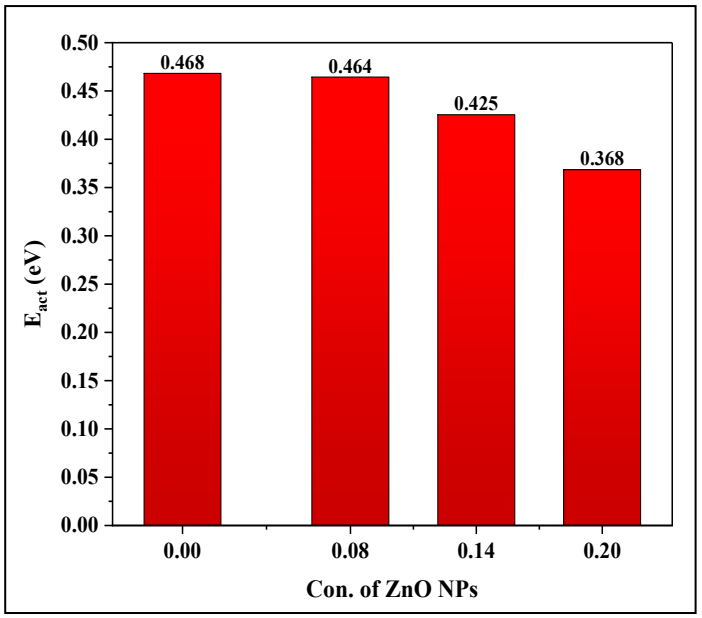

Figure 16 shows the relationship between ZnO nanoparticle concentration (wt.%) conductivity of direct current (D.C.) in CuO/ZnO thin films, as well as their activation energy.

3.6 Application of (CuO/ZnO) Thin Films as Photodetector

Photocurrent represented an important parameter that affected spectral responsivity and the linearity of detector properties. Figure 17 illustrates investigating the I-V properties of devices made of CuO and CuO/ZnO nanocomposites at room temperature, in an atmosphere with a 3V bias voltage, and under both dark and UV light conditions. A tungsten lamp with a power of 70 mW/cm² and a wavelength of 365 nm was used to measure the photocurrent, also with a 3V applied bias voltage. The photocurrent of all samples in Figure 17 of the photodetector under forward bias is attributed to enhancements in the structural characteristics of the thin film. This results in a minimal energy gap, necessitating low energy for electrons to traverse the gap. Consequently, observe that the photocurrent is elevated following the augmentation of ZnO nanoparticle ratios [42].

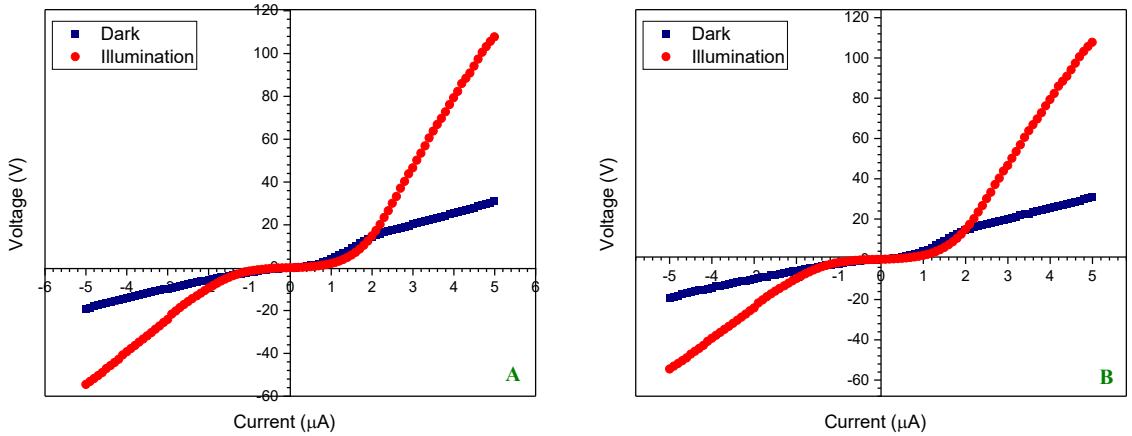

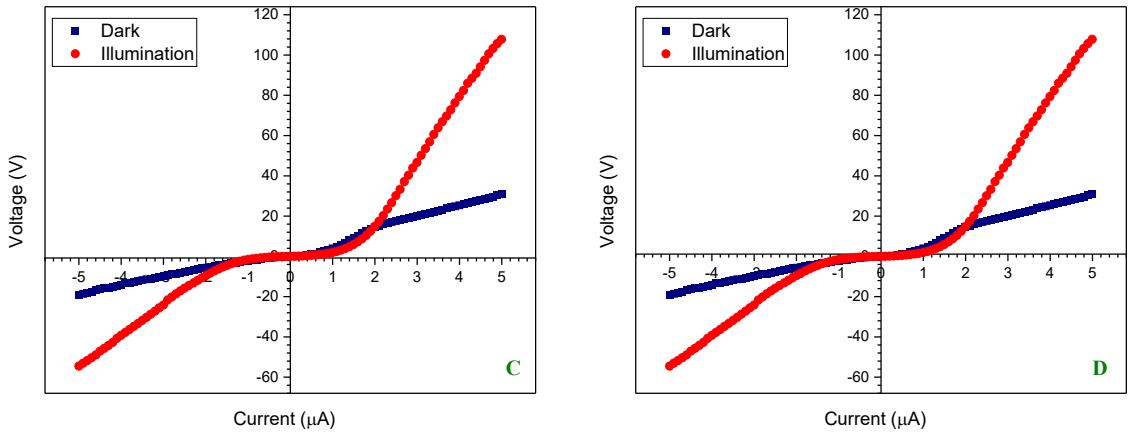

Figure 17 I-V characteristics in both dark and illuminated conditions for A: Pure CuO NPs, B: (0.08wt.%)ZnO, C:(0.14wt.%) ZnO and D:(0.20wt.%)ZnO photodetector.

Figure 18 displays the time-current graph of the thin films exposed to 26 mW/cm² white LED light with a bias voltage of 3V. This voltage was the one that revealed photovoltaic activity. A photocurrent is generated when the energy of the photons that enter the material is high enough to generate an electric field. Saturation currents of 408.87 μA, 651.16 μA, 349.98 μA, and 481.13 μA were shown in Figure 18, respectively. The electric field produces a photocurrent under a 3V applied voltage, which is used to augment the bias current. The result was an increase in the saturation current to 481.13 μA [56].

Figure 18 shows that the highest sensitivity (S%) was about 81.01% at a response time and a recovery time of 1.141 s and 0.709 s respectively at a concentration (0.20 wt.%) of ZnO. The significant figures of merit include responsivity (R_λ) and external quantum efficiency (EQE), detectivity (D), photosensitivity (S), and the times of response and recovery of photodetectors at 3 V bias are summarized in Table 2.

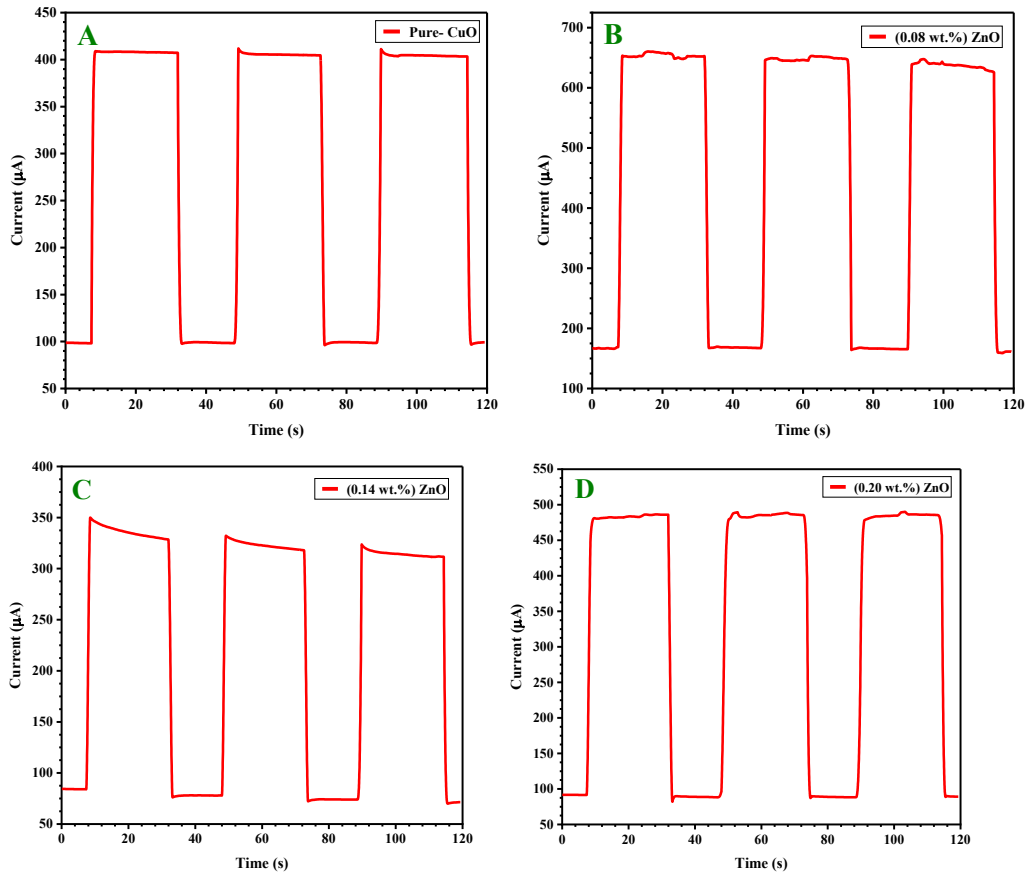

Figure 18 Photocurrent response of (CuO/ZnO) NCs A: Pure CuO, B: (0.08wt.%)ZnO, C: (0.14wt.%) ZnO and D:(0.20wt.%) ZnO photodetector.

Table 3: Photodetector measurements at 3V.

Thin films	Response time (s)	Recovery time (s)	S (%)	R_{λ} (mA/W)	QE (%)	D* (Jones)*10^6
Pure (CuO)	0.366	0,366	76	0.16241	0.553	1.596
0.08 wt.% ZnO	1.189	168.87	74.07	0.08058	0.274	0.854
0.14 wt.% ZnO	0.365	0.367	76.03	0.01851	0.063	0.117
0.20 wt.% ZnO	1.142	0.709	81.01	0.08405	0.286	0.974

4. CONCLUSIONS

In summary, CuO/ZnO nanocomposite thin films were effectively synthesized by the thermal evaporation method, thereafter subjected to annealing at 400 °C. Structural, morphological, optical, and electrical analyses validated the creation of well-defined nanocomposites exhibiting enhanced capabilities. Doping with ZnO increased surface roughness, optical absorption, and decreased the direct energy band gap, while simultaneously enhancing electrical conductivity and photodetection capability. The nanocomposites exhibited a notable photocurrent response, elevated sensitivity, and quick recovery time, particularly at a ZnO doping concentration of 0.20 wt.%. The results indicate that CuO/ZnO nanocomposites are viable options for effective UV photodetector applications.

5. ACKNOWLEDGEMENTS

To the Physics Department and the University of Babylon, we are eternally grateful for the invaluable support they provided during the course of our undertaking.

REFERENCES

[1] S. Mostafa Hosseinpour-Mashkani, M. Maddahfar, A. Sobhani-Nasab, Novel silver-doped NiTiO3: auto-combustion synthesis, characterization and photovoltaic measurements, South African J. Chem. 70 (2017) 44–48. https://doi.org/10.17159/0379-4350/2017/v70a7.

[2] P.P. Magar, V.S. Kadam, S.F. Mulla, A. V. Shaikh, H.M. Pathan, Copper and iron doped zinc oxide: chemical synthesis, characterization and their properties, J. Mater. Sci. Mater. Electron. 27 (2016) 12287–12290. https://doi.org/10.1007/s10854-016-4835-4.

[3] J. Teizer, M. Venugopal, W. Teizer, J. Felkl, Nanotechnology and Its Impact on Construction: Bridging the Gap between Researchers and Industry Professionals, J. Constr. Eng. Manag. 138 (2012) 594–604. https://doi.org/10.1061/(ASCE)CO.1943-7862.0000467.

[4] M.C. Roco, R.S. Williams, P. Alivisatos, Nanotechnology Research Directions: IWGN Workshop Report, Springer Netherlands, Dordrecht, 2000. https://doi.org/10.1007/978-94-015-9576-6.

[5] K.P. Chong, Nano Science and Engineering in Mechanics and Materials, in: Materials (Basel)., ASMEDC, 2003: pp. 273–281. https://doi.org/10.1115/IMECE2003-43239.

[6] M. Patel, S. Mishra, R. Verma, D. Shikha, Synthesis of ZnO and CuO nanoparticles via Sol gel method and its characterization by using various technique, Discov. Mater. 2 (2022). https://doi.org/10.1007/s43939-022-00022-6.

[7] N.A. Ibrahim, Nanomaterials for Antibacterial Textiles, in: Nanotechnol. Diagnosis, Treat. Prophyl. Infect. Dis., Elsevier, 2015: pp. 191–216. https://doi.org/10.1016/B978-0-12-801317-5.00012-8.

[8] Z. Yang, H. Peng, W. Wang, T. Liu, Crystallization behavior of poly(ε-caprolactone)/layered double hydroxide nanocomposites, J. Appl. Polym. Sci. 116 (2010) 2658–2667. https://doi.org/10.1002/app.31787.

[9] S. Murthy, P. Effiong, C.C. Fei, Metal oxide nanoparticles in biomedical applications, in: Met. Oxide Powder Technol., Elsevier, 2020: pp. 233–251. https://doi.org/10.1016/B978-0-12-817505-7.00011-7.

[10] S. Ibrahim, Y.M. Hamdy, H. Darwish, A.A. Ali, Effect of CuO doping on structural features, optical absorption and photoluminescence behavior of ZnO-based glasses, J. Mater. Sci. Mater. Electron. 34 (2023) 1–15. https://doi.org/10.1007/s10854-023-10270-8.

[11] T. Jintakosol, P. Singjai, Effect of annealing treatment on luminescence property of MgO nanowires, Curr. Appl. Phys. 9 (2009) 1288–1292. https://doi.org/10.1016/j.cap.2009.02.014.

[12] K.K. Ostrikov, U. Cvelbar, A.B. Murphy, Plasma nanoscience: setting directions, tackling grand challenges, J. Phys. D. Appl. Phys. 44 (2011) 174001. https://doi.org/10.1088/0022-3727/44/17/174001.

[13] M.K. Mohammed, T.N. Khudhair, K.S. Sharba, A. Hashim, Q.M. Hadi, M.H. Meteab, Tuning the Morphological and Optical Characteristics of SnO2/ZrO2 Nanomaterials Doped PEO for Promising Optoelectronics Applications, Rev. Des Compos. Des Matériaux Avancés 34 (2024) 495–503. https://doi.org/10.18280/rcma.340411.

[14] S. Ilican, M. Caglar, Y. Caglar, Sn doping effects on the electro-optical properties of sol gel derived transparent ZnO films, Appl. Surf. Sci. 256 (2010) 7204–7210. https://doi.org/10.1016/j.apsusc.2010.05.052.

[15] D.C. Look, Recent advances in ZnO materials and devices, Mater. Sci. Eng. B 80 (2001) 383–387. https://doi.org/10.1016/S0921-5107(00)00604-8.

[16] J.Y. Park, D.E. Song, S.S. Kim, An approach to fabricating chemical sensors based on ZnO nanorod arrays, Nanotechnology 19 (2008) 105503. https://doi.org/10.1088/0957-4484/19/10/105503.

[17] M.H. Asif, A. Fulati, O. Nur, M. Willander, C. Brännmark, P. Strålfors, S.I. Börjesson, F. Elinder, Functionalized zinc oxide nanorod with ionophore-membrane coating as an intracellular Ca2+ selective sensor, Appl. Phys. Lett. 95 (2009). https://doi.org/10.1063/1.3176441.

[18] F. Hussain, M. Meteab, Nuclear reaction analyses for green chemistry: Evaluating environmental safety in charged particle interactions, E3S Web Conf. 614 (2025) 04025. https://doi.org/10.1051/e3sconf/202561404025.

[19] Ü. Özgür, D. Hofstetter, H. Morkoç, ZnO Devices and Applications: A Review of Current Status and Future Prospects, Proc. IEEE 98 (2010) 1255–1268. https://doi.org/10.1109/JPROC.2010.2044550.

[20] A.B. Djurišić, A.M.C. Ng, X.Y. Chen, ZnO nanostructures for optoelectronics: Material properties and device applications, Prog. Quantum Electron. 34 (2010) 191–259. https://doi.org/10.1016/j.pquantelec.2010.04.001.

[21] M.H. Meteab, A. Hashim, B.H. Rabee, Synthesis and Structural Properties of (PS–PC/Co2O3–SiC) Nanocomposites for Antibacterial Applications, Nanosistemi, Nanomater. Nanotehnologii 21 (2023) 0451–0460. https://doi.org/10.15407/nnn.21.02.451.

[22] J. Lillo-Ramiro, J.M. Guerrero-Villalba, M. de L. Mota-González, F.S.A.- Tostado, G. Gutiérrez-Heredia, I. Mejía-Silva, A.C.- Castillo, Optical and microstructural characteristics of CuO thin films by sol gel process and introducing in non-enzymatic glucose biosensor applications, Optik (Stuttg). 229 (2021) 166238. https://doi.org/10.1016/j.ijleo.2020.166238.

[23] R. Nayak, F.A. Ali, D.K. Mishra, D. Ray, V.K. Aswal, S.K. Sahoo, B. Nanda, Fabrication of CuO nanoparticle: An efficient catalyst utilized for sensing and degradation of phenol, J. Mater. Res. Technol. 9 (2020) 11045–11059. https://doi.org/10.1016/j.jmrt.2020.07.100.

[24] P. V. Raghavendra, J.S. Bhat, N.G. Deshpande, Visible light sensitive cupric oxide metal-semiconductor-metal photodetectors, Superlattices Microstruct. 113 (2018) 754–760. https://doi.org/10.1016/j.spmi.2017.12.014.

[25] Y.-G. Lin, Y.-K. Hsu, S.-Y. Chen, L.-C. Chen, K.-H. Chen, Microwave-activated CuO nanotip/ZnO nanorod nanoarchitectures for efficient hydrogen production, J. Mater. Chem. 21 (2011) 324–326. https://doi.org/10.1039/C0JM03022H.

[26] J.X. Wang, X.W. Sun, Y. Yang, K.K.A. Kyaw, X.Y. Huang, J.Z. Yin, J. Wei, H.V. Demir, Free-standing ZnO–CuO composite nanowire array films and their gas sensing properties, Nanotechnology 22 (2011) 325704. https://doi.org/10.1088/0957-4484/22/32/325704.

[27] X. Zhao, P. Wang, B. Li, CuO/ZnO core/shell heterostructure nanowire arrays: synthesis, optical property, and energy application, Chem. Commun. 46 (2010) 6768. https://doi.org/10.1039/c0cc01610a.

[28] X. Wang, G. Xi, S. Xiong, Y. Liu, B. Xi, W. Yu, Y. Qian, Solution-Phase Synthesis of Single-Crystal CuO Nanoribbons and Nanorings, Cryst. Growth Des. 7 (2007) 930–934. https://doi.org/10.1021/cg060798j.

[29] Z.L. Wang, The new field of nanopiezotronics, Mater. Today 10 (2007) 20–28. https://doi.org/10.1016/S1369-7021(07)70076-7.

[30] Z. Liu, H. Bai, S. Xu, D.D. Sun, Hierarchical CuO/ZnO “corn-like” architecture for photocatalytic hydrogen generation, Int. J. Hydrogen Energy 36 (2011) 13473–13480. https://doi.org/10.1016/j.ijhydene.2011.07.137.

[31] Q. Simon, D. Barreca, A. Gasparotto, CuO/ZnO Nanocomposites Investigated by X-ray Photoelectron and X-ray Excited Auger Electron Spectroscopies, Surf. Sci. Spectra 17 (2010) 93–101. https://doi.org/10.1116/11.20111002.

[32] M. Jafari, H. Eshghi, High self-powered UV–Visible photoresponse in ZnO/CuO heterostructure photodetectors, the influence of ZnO window layer thickness, Opt. Mater. (Amst). 142 (2023) 113975.

https://doi.org/10.1016/j.optmat.2023.113975.

[33] N. Alwadai, S. Mitra, M.N. Hedhili, H. Alamoudi, B. Xin, N. Alaal, I.S. Roqan, Enhanced-Performance Self-Powered Solar-Blind UV-C Photodetector Based on n-ZnO Quantum Dots Functionalized by p-CuO Micro-pyramids, ACS Appl. Mater. Interfaces 13 (2021) 33335–33344. https://doi.org/10.1021/acsami.1c03424.

[34] S.B. Wang, C.H. Hsiao, S.J. Chang, K.T. Lam, K.H. Wen, S.C. Hung, S.J. Young, B.R. Huang, A CuO nanowire infrared photodetector, Sensors Actuators A Phys. 171 (2011) 207–211. https://doi.org/10.1016/j.sna.2011.09.011.

[35] F. Urbach, The Long-Wavelength Edge of Photographic Sensitivity and of the Electronic Absorption of Solids, Phys. Rev. 92 (1953) 1324. https://doi.org/10.1103/PhysRev.92.1324.

[36] J. Tauc, Optical Properties of Amorphous Semiconductors BT - Amorphous and Liquid Semiconductors, in: J. Tauc (Ed.), Springer US, Boston, MA, 1974: pp. 159–220. https://doi.org/10.1007/978-1-4615-8705-7_4.

[37] S. Arrhenius, Über die Reaktionsgeschwindigkeit bei der Inversion von Rohrzucker durch Säuren, Zeitschrift Für Phys. Chemie 4 (1889) 226–248.

[38] A. Costas, C. Florica, N. Preda, A. Kuncser, I. Enculescu, Photodetecting properties of single CuO–ZnO core–shell nanowires with p–n radial heterojunction, Sci. Rep. 10 (2020) 1–12. https://doi.org/10.1038/s41598-020-74963-4.

[39] S. Noothongkaew, O. Thumthan, K.S. An, UV-Photodetectors based on CuO/ZnO nanocomposites, Mater. Lett. 233 (2018) 318–323. https://doi.org/10.1016/j.matlet.2018.09.024.

[40] M.C. Morris, Standard X-ray diffraction powder patterns: Section 16--data for 86 substances, Department of Commerce, National Bureau of Standards, 1979.

[41] N. Al Armouzi, M. Manoua, Y. Ghanam, H.S. Hilal, A. Liba, M. Mabrouki, Enhancement of p-CuO/n-ZnO Heterojunction Photovoltaic Characteristics by Preparation Route and Sn Doping, J. Electron. Mater. 53 (2024) 3398–3412. https://doi.org/10.1007/s11664-024-11084-y.

[42] A.H.O. Alkhayatt, A. Abed Abdul Wahab H, A. Ali Abdulhussein Hameed, Optical band gap Modification and Photodetector Properties of Au NPs Doped CuZnS Thin Films, J. Kufa-Physics 10 (2018) 95–107. https://doi.org/10.31257/2018/JKP/100115.

[43] R.O. Yathisha, Y. Arthoba Nayaka, P. Manjunatha, H.T. Purushothama, M.M. Vinay, K. V. Basavarajappa, Study on the effect of Zn 2+ doping on optical and electrical properties of CuO nanoparticles, Phys. E Low-Dimensional Syst. Nanostructures 108 (2019) 257–268. https://doi.org/10.1016/j.physe.2018.12.021.

[44] S.T. Abdulredha, N.A. Abdulrahman, Cu-ZnO nanostructures synthesis and characterization, Iraqi J. Sci. 62 (2021) 708–717. https://doi.org/10.24996/ijs.2021.62.3.1.

[45] R. Grazziotin-Soares, M.H. Nekoofar, T.E. Davies, A. Bafail, E. Alhaddar, R. Hübler, A.L.S. Busato, P.M.H. Dummer, Effect of bismuth oxide on white mineral trioxide aggregate: chemical characterization and physical properties, Int. Endod. J. 47 (2014) 520–533. https://doi.org/10.1111/IEJ.12181.

[46] K. Mubeen, A. Irshad, A. Safeen, U. Aziz, K. Safeen, T. Ghani, K. Khan, Z. Ali, I. ul Haq, A. Shah, Band structure tuning of ZnO/CuO composites for enhanced photocatalytic activity, J. Saudi Chem. Soc. 27 (2023) 101639. https://doi.org/https://doi.org/10.1016/j.jscs.2023.101639.

[47] F.P. Koffyberg, F.A. Benko, A photoelectrochemical determination of the position of the conduction and valence band edges of p-type CuO, J. Appl. Phys. 53 (1982) 1173–1177. https://doi.org/10.1063/1.330567.

[48] A. Razzaq Abdul Ridha, N.A. Al-Isawi, Studying the effect of annealing temperatures on the optical properties of CdS:1% Cu nanoparticles thin films prepared by thermal evaporation technique, J. Phys. Conf. Ser. 1234 (2019) 012029. https://doi.org/10.1088/1742-6596/1234/1/012029.

[49] F. Teimoori, K. Khojier, N.Z. Dehnavi, On the Dependence of H2 Gas Sensitivity of ZnO thin Films on Film Thickness, Procedia Mater. Sci. 11 (2015) 474–479. https://doi.org/10.1016/j.mspro.2015.11.061.

[50] T.T. Liu, M. hua Wang, H.P. Zhang, Synthesis and Characterization of ZnO/Bi2O3 Core/Shell Nanoparticles by the Sol–Gel Method, J. Electron. Mater. 45 (2016) 4412–4417. https://doi.org/10.1007/S11664-016-4568-4.

[51] S. Indris, P. Heitjans, M. Ulrich, A. Bunde, AC and DC Conductivity in Nano- and Microcrystalline Li2O : B2O3 Composites: Experimental Results and Theoretical Models, Zeitschrift Fur Phys. Chemie 219 (2005) 89–103. https://doi.org/10.1524/zpch.219.1.89.55015.

[52] A. Hashim, Q. Hadi, Structural, electrical and optical properties of (biopolymer blend/titanium carbide) nanocomposites for low cost humidity sensors, J. Mater. Sci. Mater. Electron. 29 (2018) 11598–11604. https://doi.org/10.1007/s10854-018-9257-z.

[53] H.S. Suhail, A.R. Abdulridha, Investigation of the Morphological, Optical, and D.C Electrical Characteristics of Synthesized (Bi2O3/ZnO) Nanocomposites, as Well as Their Potential Use in Hydrogen Sulfide Gas Sensor, Trans. Electr. Electron. Mater. 24 (2023) 205–216. https://doi.org/10.1007/s42341-023-00436-w.

[54] A. Sawalha, M. Abu-Abdeen, A. Sedky, Electrical conductivity study in pure and doped ZnO ceramic system, Phys. B Condens. Matter 404 (2009) 1316–1320. https://doi.org/10.1016/j.physb.2008.12.017.

[55] A. Sawalha, M. Abu-Abdeen, A. Sedky, Preparation and Characterization of Thin Films Bismuth(III) Oxide/Zinc Oxide Nanostructures Prepared by Thermal Evaporation Technique as Gas Sensor Applications, Phys. B Condens. Matter 404 (2009) 1316–1320. https://doi.org/10.1007/s42341-023-00490-4.

[56] E. Aslan, Improving the device performance of CuO-based self-powered photodetectors by cobalt doping, J. Phys. Chem. Solids 191 (2024) 112032. https://doi.org/10.1016/j.jpcs.2024.112032.